micromachines

MDPI

Article

A Novel Self-Temperature Compensation Method for Mode-Localized Accelerometers

Pengcheng Cai [1,2], Xingyin Xiong [1,*], Kunfeng Wang [1,2], Liangbo Ma [1,2], Zheng Wang [3], Yunfei Liu [1,2] and Xudong Zou [1,2,*]

[1] State Key Laboratory of Transducer Technology, Aerospace Information Research Institute, Chinese Academy of Sciences, Beijing 100190, China; caipengcheng16@mails.ucas.ac.cn (P.C.); wangkunfeng17@mails.ucas.ac.cn (K.W.); maliangbo19@mails.ucas.ac.cn (L.M.); liuyunfei17@mails.ucas.ac.cn (Y.L.)

[2] School of Electronic, Electrical and Communication Engineering, University of Chinese Academy of Sciences, Beijing 100049, China

[3] QiLu Aerospace Information Research Institute, Jinan 250101, China; wangzheng02@aircas.cn

[*] Correspondence: xyxiong@mail.ie.ac.cn (X.X.); zouxd@aircas.ac.cn (X.Z.); Tel.: +86-10-58887261 (X.X.); +86-10-58887528 (X.Z.)

Abstract: Mode-localized sensing paradigms applied to accelerometers have recently become popular research subjects. However, the output of mode-localized accelerometers is influenced by environment temperature due to the difference in the thermal properties of the coupling resonators and the temperature dependence of coupling stiffness. To improve the performance of mode-localized accelerometers against temperature, we proposed an in situ self-temperature compensation method by utilizing the resonant frequency besides of amplitude ratios, which can be implied online. Experimental results showed that there were nearly 79-times and 87-times improvement in zeros bias and scale factor, respectively.

Keywords: 2-DoF; mode-localized accelerometer; compensation

Citation: Cai, P.; Xiong, X.; Wang, K.; Ma, L.; Wang, Z.; Liu, Y.; Zou, X. A Novel Self-Temperature Compensation Method for Mode-Localized Accelerometers. *Micromachines* **2022**, *13*, 437. https://doi.org/10.3390/mi13030437

Academic Editor: Aiqun Liu

Received: 16 February 2022
Accepted: 9 March 2022
Published: 13 March 2022

Publisher's Note: MDPI stays neutral with regard to jurisdictional claims in published maps and institutional affiliations.

Copyright: © 2022 by the authors. Licensee MDPI, Basel, Switzerland. This article is an open access article distributed under the terms and conditions of the Creative Commons Attribution (CC BY) license (https://creativecommons.org/licenses/by/4.0/).

1. Introduction

MEMS (Microelectromechanical systems) accelerometers have the advantages of small size, light weight, low power consumption and low cost [1]; thus, they are widely used in the fields of inertial navigation, medical consumer electronics and automotives [2,3]. Among various kinds of MEMS accelerometers, silicon resonant accelerometers are promising for high sensitivity, large linear range, low bias instability and so on [4–7].

Over the past few years, the mode-localized sensing paradigm based on weakly coupled resonators (WCRs) has been researched and applied to various kinds of sensors including accelerometers for its ultra-high sensitivity [8–14] and the suppression of common mode noises [15–19] with the output metric of the amplitude ratio. In a sensor using WCRs, weaker coupling strength means higher sensitivity. Some works have made efforts to achieve lower coupling stiffness, among which the electrically stiffness coupling and mechanical coupling structure are widely used. Compared with the scheme of electrical stiffness coupling, coupling structures lack the noise from a coupling voltage. As there is a difference in the properties of the coupled resonators, mode-localized accelerometers still suffer from the influence of temperature since there would be thermal perturbation as temperature fluctuates. Furthermore, as the Young's modulus of the silicon material is very sensitive to temperature, mechanical coupling stiffness is temperature-dependent, making the temperature performance worse. To improve the temperature performance of MEMS accelerometers, some methods were proposed including active temperature control [20–23], temperature compensation [24–26] and less temperature sensitivity structure [27]. The active temperature control scheme requires complex temperature control

systems and higher power consumption. The scheme of reducing the temperature sensitivity by structure design can only achieve a limited improvement. Therefore, a passive temperature compensation scheme is widely used for its simplicity. One of the passive temperature compensation methods is to make a compensated result with the output of the accelerometer and the temperature captured by an additional thermometer or temperature sensitive element. Another way is to implement self-temperature compensation by the two outputs from a differential structure of resonant accelerometer [28,29]. As there is no need for additional temperature measurement in the second way, the problem of thermal lag between the thermometer and the accelerometer is alleviated. However, this scheme of self-temperature compensation proposed for differential structure is not in situ exactly, as there is distance between the differential resonators. Furthermore, there have been less studies on the temperature compensation for mode-localized accelerometers.

In this article, we proposed a self-temperature compensation method which is an in situ compensation way for a two degree-of-freedom (2-DoF) mode-localized mechanically coupled accelerometer. To the best of our knowledge, this is the first work proposing a in situ self- temperature compensation method for 2-DoF mode-localized accelerometers by using amplitude ratios and resonant frequency together. A neural network was trained to study the relationship between the parameters with amplitude ratios and resonant frequency under different temperature. With a real-time measurement on resonant frequency besides of amplitude ratio, the proposed method for a 2-DoF mode-localized accelerometer can be applied online.

2. Two-DoF WCRs Accelerometer

A simplified model of mode localized accelerometer based on a 2-DoF weakly coupled resonator is shown in Figure 1. Ideally the mass and the stiffness of the two resonators are initially symmetric: i.e., $m_1 = m_2 = m$, $k_1 = k$, $k_2 = k + \Delta k$, where m_1, m_2 represent the effective mass of each resonator and k_1, k_2 represent the effective stiffness of each resonator while Δk represents the stiffness perturbation, k_c represents the coupling stiffness.

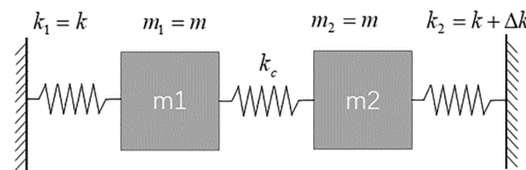

Figure 1. Mass–spring–damper model of a 2-DoF WCRs with external perturbation.

Without considering damping terms and driving force the motion of the system can be formulated as

$$\begin{bmatrix} m & 0 \\ 0 & m \end{bmatrix} \begin{bmatrix} \ddot{x}_1 \\ \ddot{x}_2 \end{bmatrix} + \begin{bmatrix} k + k_c & -k_c \\ -k_c & k + k_c + \Delta k \end{bmatrix} \begin{bmatrix} x_1 \\ x_2 \end{bmatrix} = \begin{bmatrix} 0 \\ 0 \end{bmatrix} \tag{1}$$

where x_1 and x_2 are the displacements of the two masses. With using the resonant frequency of first mode without structural perturbation $\omega_0 = \sqrt{k/m}$, the resonant radian frequencies ω_i (i = 1, 2) and amplitude ratios u_i (i = 1, 2) of the two modes can be derived as:

$$\omega_i = \left(\sqrt{1 + \frac{1}{k}\left(k_c + \frac{\Delta k}{2} \mp \frac{1}{2}\sqrt{\Delta k^2 + 4k_c^2} \right)} \right) \omega_0 \tag{2}$$

$$u_{i-12} = \frac{x_{i1}}{x_{i2}} = \frac{\Delta k \pm \sqrt{\Delta k^2 + 4k_c^2}}{2k_c} \tag{3}$$

$$u_{i-21} = \frac{x_{i2}}{x_{i1}} = -\frac{\Delta k \mp \sqrt{\Delta k^2 + 4k_c^2}}{2k_c} \tag{4}$$

As the perturbation varies, the amplitude ratio u_{i-12} in the first vibrational mode (i = 1) goes from good linearity to strong nonlinearity, while he amplitude ratio u_{i-12} in the second vibrational mode (i = 2) is to the opposite. This trend of amplitude ratios u_{i-21} (i = 1, 2) is opposite to the amplitude ratio u_{i-12} (i = 1, 2). Work [30] proposed a method to enhance the linearity of WCRs by using output metric based on the subtraction of reciprocal amplitude ratios. This method can be implemented by simple calculation of the amplitude ratios from one WCRs. The method can be formulated as (i = 1, 2):

$$u_{oi} = u_{i-12} - u_{i-21} = \frac{x_{i1}}{x_{i2}} - \frac{x_{i2}}{x_{i1}} = \frac{\Delta k}{k_c} \quad (5)$$

where u_{oi} (i = 1, 2) is the linearity-enhanced output metric. By using linearity-enhanced output metric, a larger linear range can be achieved.

The schematic of our mode localized accelerometer is shown in Figure 2. The two clamped-clamped (CC) resonators are coupled with each other by a micro-lever coupler. The two resonators are driven and sensed by parallel-plate capacitors at two sides of the resonators. The proof mass is suspended and connected to one of the CC resonators through a pair of micro-lever force amplifiers. When an acceleration is applied along the sensitivity axis direction, a corresponding perturbation is made through the micro-lever force amplifiers by the proof mass. The amplitude ratios of WCRs will change with the perturbation.

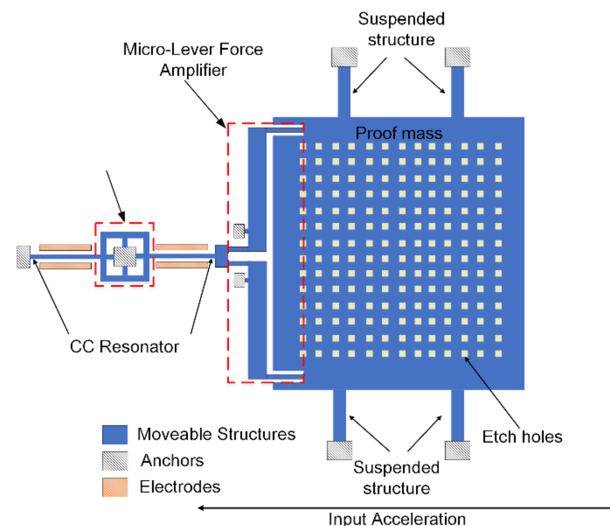

Figure 2. The schematic of the mode localized accelerometer.

The geometrical dimensions of the DETF-CC WCRs mode localized accelerometer are summarized in Table 1.

Table 1. Parameters of the accelerometer.

Parameter	Value
Device thickness	40 µm
Length of CC resonant beam	400 µm
Width of CC resonant beam	7 µm
Gap of resonant beam	2 µm
Quality of proof mass	1.50 mg
Quality factor	15,600
Glass thickness	50 µm

We made verification of the linearity-enhanced output metric on our mode-localized accelerometer by taking a Finite Element Multiphysics (FEM) simulation. In the accelerome-

ter, out-of-phase mode and in-phase mode were worked as the first mode (i = 1) and second mode (i = 2) as shown in Figure 3a,b, respectively. The amplitude ratios of the two modes and their linearity-enhanced output metric are shown in Figure 3a,b, respectively as well.

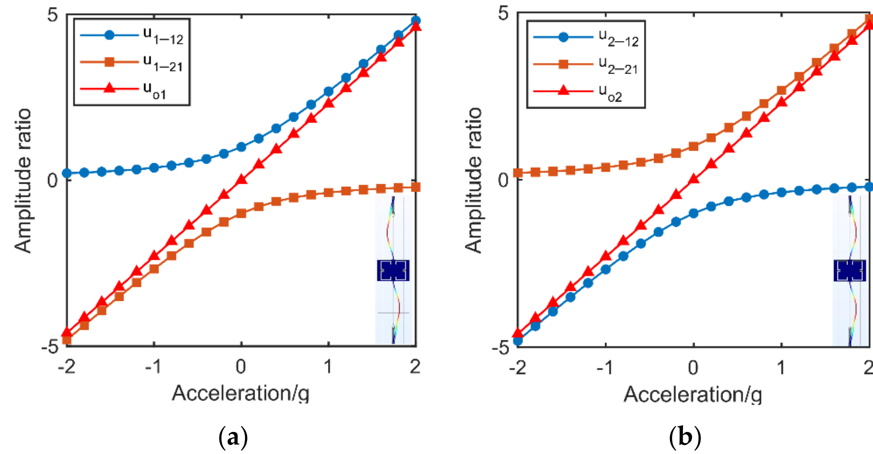

Figure 3. (**a**) Mode shape, amplitude ratios and linearity-enhanced output metric of the first mode. (**b**) Mode shape, amplitude ratios and linearity-enhanced output metric of the second mode.

3. Temperature Dependence Analysis of 2-DoF Accelerometer

3.1. The Dependence of Linearity-Enhanced Output Metric on Temperature

As the temperature changes, the difference in the thermal expansion coefficient between the materials and the residual stress generated in the fabrication process will cause an extra thermal perturbation on the WCRs besides the acceleration applied, inducing a bias drift with temperature on the output of mode-localized accelerometers. Furthermore, the coupling stiffness is also temperature dependent, especially in a mechanical coupling structure since the Young's modulus of the silicon material will change with temperature. This effect will induce the sensitivity fluctuated with the temperature. Thus, the linearity-enhanced output metric (i = 1, 2) of a 2-DoF mode-localized accelerometer can be expressed as Equation (6) with considering of the impact caused by the temperature.

$$u_{oi}(T) = \frac{\Delta k_a}{k_c(T)} + \frac{\Delta k_T(T)}{k_c(T)} \quad (6)$$

where Δk_a is the perturbation caused by acceleration and $\Delta k_T(T)$ is the perturbation induced by internal thermal stress at the temperature T, while $k_c(T)$ is the coupling stiffness at temperature T.

3.2. The Dependence of Frequency on Temperature

The resonant frequencies of the two vibrational modes of a WCRs is also influenced by the temperature. Besides of the internal thermal stress and coupling stiffness, the changes in stiffness of the coupling resonators also make the resonant radian frequencies (i = 1, 2) temperature dependent as shown in Equation (7), where $\omega_0(T) = \sqrt{\frac{k(T)}{m}}$.

$$\omega_i(T) = \left(\sqrt{1 + \frac{1}{k(T)}(k_c(T) + \frac{\Delta k_a + \Delta k_T}{2} \mp \frac{1}{2}\sqrt{(\Delta k_a + \Delta k_T)^2 + 4k_c^2(T)}}\right)\omega_0(T) \quad (7)$$

4. The Method of Temperature Compensation

We took the linearity-enhanced output metric to measure the acceleration. The relationship on the linearity-enhanced output metrics and acceleration is expressed as (i = 1, 2):

$$u_{oi} = S_{Fi}a + Bias_i \quad (8)$$

Since the sensitivity and bias against external stiffness perturbation of u_{oi} i = 1, 2) are temperature dependent, the scale factor S_{Fi} and bias $Bias_i$ against acceleration are also temperature dependent in a mode-localized accelerometer (i = 1, 2). Therefore, the main goal is to make compensation for S_{Fi} and $Bias_i$ (i = 1, 2).

According to Equations (2)–(4), the relationship between resonant frequencies and amplitude ratios (i = 1, 2) can be derived as:

$$\omega_i = \left[\sqrt{1 + \frac{k_c(T)}{k(T)}(1 + \frac{]}{u_{i-12}})}\right]\omega_0(T) = \left[\sqrt{1 + \frac{k_c(T)}{k(T)}(1 - u_{i-21})}\right]\omega_0(T) \tag{9}$$

According to Equation (9), it is known that the relationship between resonant radian frequencies and amplitude ratios (i = 1, 2) is decided by the parameters of the coupling resonators which are dependent on the temperature. As the perturbation is consisted in the amplitude ratios and there is no term consisting of the perturbation made by acceleration applied, the relationship is independent on the applied acceleration. An FEM simulation was taken to prove the issues. As shown in Figure 4, by applying different acceleration over the range from −1 g to 1 g with a step of 0.1 g at 300 K and 310 K, respectively, simulation points were gotten and drawn in Figure 4. The fitting curves between resonant frequencies and amplitude ratios (i = 1) at 300 K and 310 K have the same format with Equation (9), with a coefficient of determination of $R^2 = 1$. Though the amplitude ratios changes with the acceleration applied, the relationship is fixed under a certain temperature.

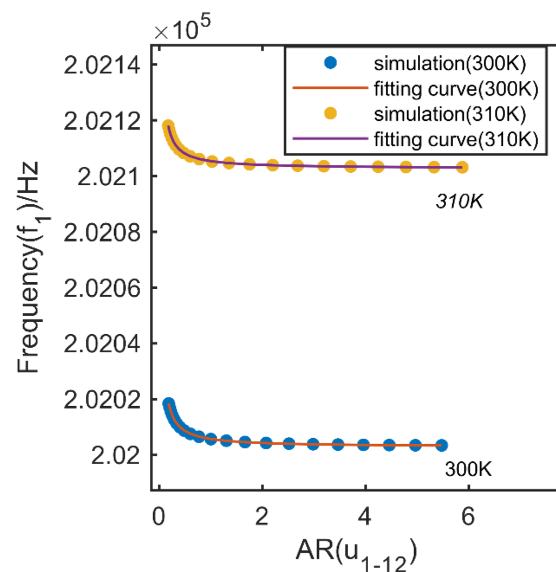

Figure 4. FEM simulation for the relationship between amplitude and resonant frequency under different temperature.

By measuring resonant frequency f_i, amplitude ratios u_{i-12} and u_{i-21} (i = 1, 2) at real-time, the temperature T of the coupling resonators may be inferred with ω_i and u_{i-12} or u_{i-21} and then the scale factor S_{Fi} and bias $Bias_i$ (i = 1, 2) by taking the linearity-enhanced output metric u_{oi} (i = 1, 2) at T can be inferred, which can be formulated as (i = 1, 2)

$$Bias_i(T) = G_1(f_i, u_{i-12}) = G_2(f_i, u_{i-21}) = G(f_i, u_{i-12}, u_{i-21}) \tag{10}$$

$$S_{Fi}(T) = H_1(f_i, u_{i-12}) = H_2(f_i, u_{i-21}) = H(f_i, u_{i-12}, u_{i-21}) \tag{11}$$

By taking the linearity-enhanced output metric according to Equation (5) with Equation (8), the temperature compensated result of the accelerometer can be achieved as ($i = 1, 2$)

$$a = \frac{u_{oi} - Bias_i(T)}{S_{Fi}(T)} \tag{12}$$

In this work, we use a five-layer feed-forward fitting neural network to explore G and H. The process of implementing proposed temperature compensation method consists of three steps. First, certain calibration points are measured. In this step, the amplitude ratio and resonant frequency of mode localized accelerometer with applied acceleration in full acceleration scales $(a_1, a_2, \ldots, a_n)$ under different temperature $(T_1, T_2, \ldots, T_m)$ over the full temperature range were recorded. In the second step, the scale factor S_{Fi} and bias $Bias_i$ ($i = 1, 2$) under different temperature calculated from linearity-enhanced output metric are used to train the neural network together with the amplitude ratio and resonant frequency of corresponding temperature. In this network training process, the frequency, the amplitude ratio and its reciprocal at calibration temperature T work as network inputs and the scale factor, bias at temperature T work as desired output. Third, the trained neural network is used as the temperature model of the accelerometer and got the compensated result with Equation (12). A detailed data flow of the proposed method is shown in Figure 5.

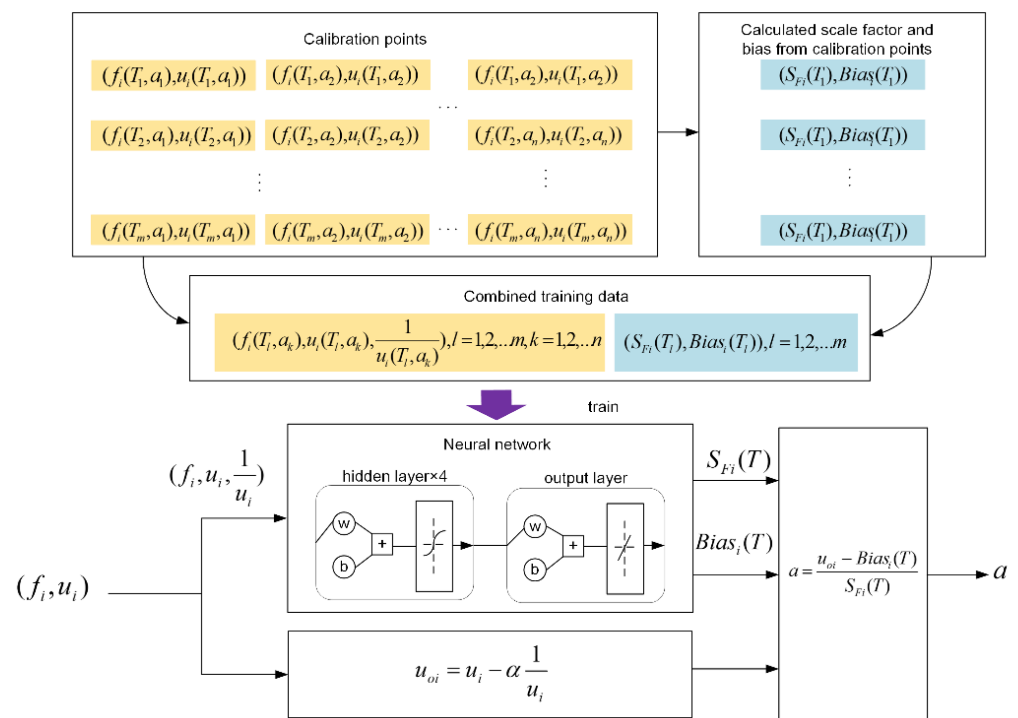

Figure 5. Data flow of the compensation process.

5. Experiment

We took experimental verification on our 2-DoF WCRs mode-localized accelerometer device. The accelerometer was fabricated by the silicon-on-glass (SOG) process. The photograph under optical microscope of the mode-localized accelerometer is shown in Figure 6.

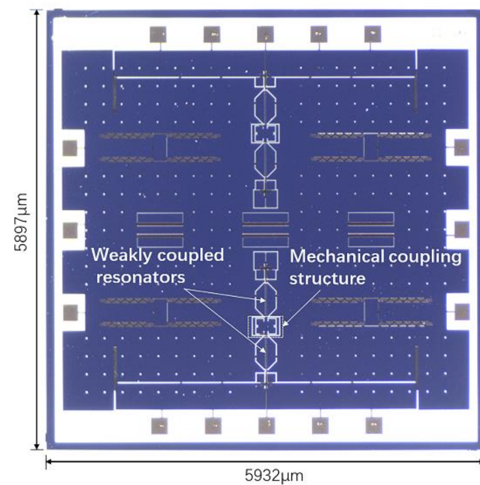

Figure 6. Photograph of mode-localized accelerometer.

In our experiment, the mode-localized accelerometer worked in in-phase or the first mode. The linearity-enhanced output metric by Equation (5) where i = 1 was taken to measure the acceleration. Applied with different accelerations, the output metrics under different temperature were shown in Figure 7. As shown in Figure 7, with the temperature varied, the zero bias and scale factor changed from 0 g, 1.08 AR/g at 300 K to −0.42 g and 1.77 AR/g at 360 K, respectively. The zero bias and scale factor were proved to be temperature dependent which is corresponding with our analysis before.

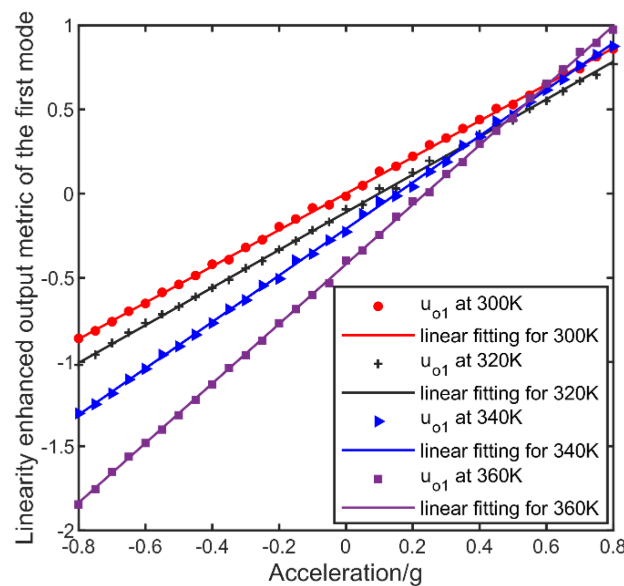

Figure 7. Data flow of the compensation process.

In the step of temperature compensation, we recorded the amplitude ratio u_{1-12}, resonant frequency with applied acceleration from −0.8 g to 0.8 g of 0.05 g step within the temperature range from 300 K to 360 K with a step of 5 K and made them as the dataset together with corresponding scale factor and bias for neural network. Then, the trained network was used to implement the compensation by the proposed method. The comparation before and after compensation was shown in Figure 8, where the bias acceleration and scale factor at 300 K were taken as the reference.

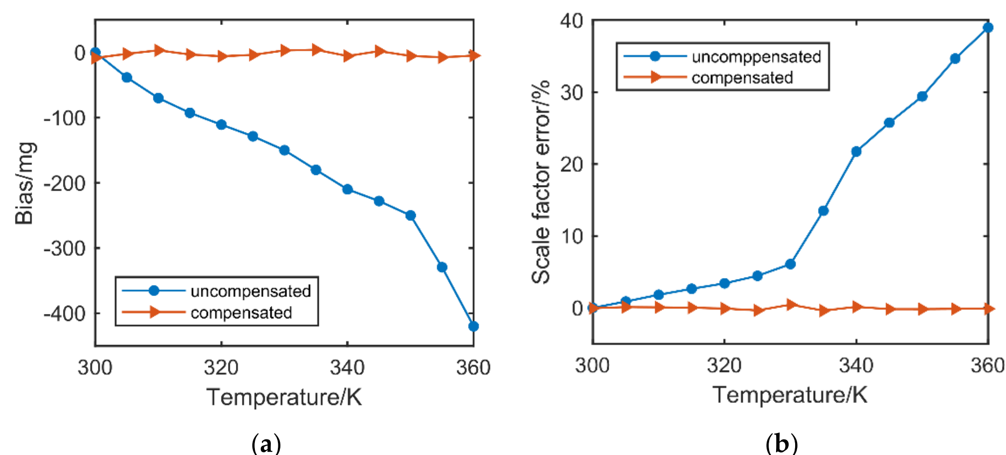

Figure 8. (**a**) Comparation on bias drifts of acceleration before and after compensation. (**b**) Comparation on errors of scale factor before and after compensation.

As shown in Figure 8a, the bias drift was decreased from 420 mg to less than 5.3 mg after compensation over the temperature range from 300 K to 360 K, which is about 79 times better than before compensation. And the scale factor error became less than 0.45% from 38.98% in the temperature range as shown in Figure 8b, achieving nearly 87 times of improvement in performance. We also made a comparison of our method with work [27] in Table 2, where work [27] decreased the influence of temperature by a good design on the structure. As shown in Table 2, both the performance in bias and scale factor against temperature were better in our work.

Table 2. Comparison with work [27].

	This Work	**[27]**
Temperature range	300 K–360 K	303 K–333 K
Bias drift	0.088 mg/K	0.22 mg/K
Scale factor over the temperature range	0.45%	0.94%

6. Conclusions

This article proposed a new method to compensate the affection of temperature fluctuation on 2-DoF mode-localized accelerometers. In the proposed method, the resonant frequency is applied to sensing temperature with the amplitude ratios of the coupled resonators itself, which may avoid the thermal lag. The method was proved to be effective and can be realized as a real-time temperature compensation for mode-localized accelerometers.

Author Contributions: Conceptualization, X.Z.; methodology, P.C. and X.X.; validation, P.C.; formal analysis, L.M.; resources, X.Z.; investigation, Z.W. and Y.L.; data curation, K.W.; writing—original draft preparation, P.C.; writing—review and editing, X.X.; supervision, X.Z.; funding acquisition, X.Z. All authors have read and agreed to the published version of the manuscript.

Funding: This research was funded by the National Key Research and Development Program of China, grant No. 2018YFB2002300.

Acknowledgments: The authors would like to thank Wuhao Yang and Zhitian Li for thier assistance with our experiments. Thanks to everyone who helped us during our work.

Conflicts of Interest: The authors declare no conflict of interest.

References

1. Weinberg, M.S.; Bernstein, J.; Borenstein, J.T.; Campbell, J.; Sohn, J.B. Micromachining inertial instruments. In *Micromachining and Microfabrication Process Technology II*; International Society for Optics and Photonics: Bellingham, WA, USA, 1996; Volume 2879, pp. 26–36.
2. Judy, M.W. Evolution of integrated inertial mems technology. In Proceedings of the Solid-State Sensors Actuator and Microsystems Workshop, 6–10 June 2004, Hilton Head Island, SC, USA; 2004; pp. 27–32.
3. Marek, J. MEMS for automotive and consumer electronics. In Proceedings of the 2010 IEEE International Solid-State Circuits Conference—(ISSCC), San Francisco, CA, USA, 7–11 February 2010.
4. Comi, C.; Corigliano, A.; Langfelder, G.; Longoni, A.; Tocchio, A.; Simoni, B. A Resonant Microaccelerometer With High Sensitivity Operating in an Oscillating Circuit. *J. Microelectromechanical Syst.* **2010**, *19*, 1140–1152. [CrossRef]
5. Seshia, A.A.; Palaniapan, M.; Roessig, T.A.; Howe, R.T.; Montague, S. A vacuum packaged surface micromachined resonant accelerometer. *J. Microelectromechanical Syst.* **2003**, *11*, 784–793. [CrossRef]
6. Omura, Y.; Nonomura, Y.; Tabata, O. New resonant accelerometer based on rigidity change. In Proceedings of the International Conference on Solid State Sensors & Actuators, Chicago, IL, USA, 19–19 June 1997.
7. Kim, S.Y.; Go, J.S.; Cho, Y.H. Design, fabrication and static test of a resonant microaccelerometer. In *ASME International Mechanical Engineering Congress and Exposition*; American Society of Mechanical Engineers: New York, NY, USA, 1997; Volume 18435, pp. 21–26.
8. Spletzer, M.; Raman, A.; Sumali, H.; Sullivan, J.P. Highly sensitive mass detection and identification using vibration localization in coupled microcantilever arrays. *Appl. Phys. Lett.* **2008**, *92*, 122. [CrossRef]
9. Manav, M.; Reynen, G.; Sharma, M.; Cretu, E.; Phani, A.S. Ultrasensitive resonant MEMS transducers with tunable coupling. In Proceedings of the 2013 Transducers & Eurosensors XXVII: The 17th International Conference on Solid-State Sensors, Actuators and Microsystems (TRANSDUCERS & EUROSENSORS XXVII), 16–20 June 2013, Barcelona, Spain; pp. 996–999.
10. Zhao, C.; Wood, G.S.; Xie, J.; Chang, H.; Pu, S.H.; Kraft, M. A Three Degree-of-Freedom Weakly Coupled Resonator Sensor With Enhanced Stiffness Sensitivity. *J. Microelectromechanical Syst.* **2016**, *25*, 38–51. [CrossRef]
11. Zhao, C.; Wood, G.S.; Xie, J.; Chang, H.; Pu, S.H.; Kraft, M. A Comparative Study of Output Metrics for an MEMS Resonant Sensor Consisting of Three Weakly Coupled Resonators. *J. Microelectromechanical Syst.* **2016**, *25*, 626–636. [CrossRef]
12. Kang, H.; Yang, J.; Chang, H. A Closed-Loop Accelerometer Based on Three Degree-of-Freedom Weakly Coupled Resonator With Self-Elimination of Feedthrough Signal. *IEEE Sens. J.* **2018**, *18*, 3960–3967. [CrossRef]
13. Zhang, H.; Li, B.; Yuan, W.; Kraft, M.; Chang, H. An Acceleration Sensing Method Based on the Mode Localization of Weakly Coupled Resonators. *J. Microelectromechanical Syst.* **2016**, *25*, 286–296. [CrossRef]
14. Peng, B.; Hu, K.; Shao, L.; Yan, H.; Li, L.; Wei, X.; Zhang, W. A Sensitivity Tunable Accelerometer Based on Series-Parallel Electromechanically Coupled Resonators Using Mode Localization. *J. Microelectromechanical Syst.* **2020**, *29*, 3–13. [CrossRef]
15. Zhang, H.; Zhong, J.; Yuan, W.; Yang, J.; Chang, H. Ambient pressure drift rejection of mode-localized resonant sensors. In Proceedings of the 2017 IEEE 30th International Conference on Micro Electro Mechanical Systems (MEMS), Las Vegas, NV, USA, 22–26 January 2017; pp. 1095–1098.
16. Thiruvenkatanathan, P.; Yan, J.; Seshia, A.A. Common mode rejection in electrically coupled MEMS resonators utilizing mode localization for sensor applications. In Proceedings of the 2009 IEEE International Frequency Control Symposium Joint with the 22nd European Frequency and Time forum, Besancon, France, 20–24 April 2009; pp. 358–363.
17. Zhong, J.; Yang, J.; Chang, H. The temperature drift suppression of mode-localized resonant sensors. In Proceedings of the 2018 IEEE Micro Electro Mechanical Systems (MEMS), Belfast, UK, 21–25 January 2018; pp. 467–470.
18. Pandit, M.; Zhao, C.; Sobreviela, G.; Seshia, A.A. Immunity to Temperature Fluctuations in Weakly Coupled MEMS Resonators. In Proceedings of the 2018 IEEE SENSORS, New Delhi, India, 28–31 October 2018; pp. 1–4.
19. Pandit, M.; Zhao, C.; Sobreviela, G.; Seshia, A. Practical Limits to Common Mode Rejection in Mode Localized Weakly Coupled Resonators. *IEEE Sens. J.* **2020**, *20*, 6818–6825. [CrossRef]
20. Xu, C.; Segovia-Fernandez, J.; Kim, H.J.; Piazza, G. Temperature-Stable Piezoelectric MEMS Resonators Using Integrated Ovens and Simple Resistive Feedback Circuits. *J. Microelectromechanical Syst.* **2017**, *26*, 187–195. [CrossRef]
21. Liu, C.; Tabrizian, R.; Ayazi, F. A $\pm$ 0.3 ppm Oven-Controlled MEMS Oscillator Using Structural Resistance-Based Temperature Sensing. *IEEE Trans. Ultrason. Ferroelectr. Freq. Control* **2018**, *65*, 1492–1499. [CrossRef] [PubMed]
22. Yang, D.; Woo, J.K.; Lee, S.; Mitchell, J.; Challoner, A.D.; Najafi, K. A Micro Oven-Control System for Inertial Sensors. *J. Microelectromechanical Syst.* **2017**, *26*, 507–518. [CrossRef]
23. Salvia, J.C.; Melamud, R.; Chandorkar, S.A.; Lord, S.F.; Kenny, T.W. Real-Time Temperature Compensation of MEMS Oscillators Using an Integrated Micro-Oven and a Phase-Locked Loop. *J. Microelectromechanical Syst.* **2010**, *19*, 192–201. [CrossRef]
24. Ng, E.J.; Ahn, C.H.; Yang, Y.; Hong, V.A.; Chiang, C.; Ahadi, E.; Ward, M.W.; Kenny, T.W. Localized, degenerately doped epitaxial silicon for temperature compensation of resonant MEMS systems. In Proceedings of the 2013 Transducers & Eurosensors XXVII: The 17th International Conference on Solid-State Sensors, Actuators and Microsystems (TRANSDUCERS & EUROSENSORS XXVII), Barcelona, Spain, 16–20 June 2013; pp. 2419–2422.
25. Li, B.; Li, C.; Zhao, Y.; Han, C.; Zhang, Q. An integrated packaged resonant accelerometer with temperature compensation. *Rev. Sci. Instrum.* **2020**, *91*, 105004. [CrossRef] [PubMed]

26. Chiang, C.; Graham, A.B.; Lee, B.J.; Ahn, C.H.; Kenny, T.W. Resonant pressure sensor with on-chip temperature and strain sensors for error correction. In Proceedings of the 2013 IEEE 26th International Conference on Micro Electro Mechanical Systems (MEMS), Taipei, Taiwan, 16–20 June 2013.
27. Kang, H.; Ruan, B.; Hao, Y.; Chang, H. A Mode-Localized Resonant Accelerometer With Self-Temperature Drift Suppression. *IEEE Sens. J.* **2020**, *20*, 12154–12165. [CrossRef]
28. Zotov, S.A.; Simon, B.R.; Trusov, A.A.; Shkel, A.M. High Quality Factor Resonant MEMS Accelerometer With Continuous Thermal Compensation. *IEEE Sens. J.* **2015**, *15*, 5045–5052. [CrossRef]
29. Li, Y.; Wang, J.; Luo, Z.; Chen, D.; Chen, J. A Resonant Pressure Microsensor Capable of Self-Temperature Compensation. *Sensors* **2015**, *15*, 10048–10058. [CrossRef] [PubMed]
30. Guo, X.; Yang, B.; Li, C.; Liang, Z. Enhancing Output Linearity of Weakly Coupled Resonators by Simple Algebraic Operations. *Sens. Actuators A Phys.* **2021**, *325*, 112696. [CrossRef]